Final Draft
of the original manuscript:

Philipp, A.; Eichinger, J.F.; Aydin, R.C.; Georgiadis, A.; Cyron, C.J.; Retsch, M.:

The accuracy of laser flash analysis explored by finite element method and numerical fitting.

In: Heat and Mass Transfer. Vol. 56 (2020) 811 - 823.
First published online by Springer: 11.10.2019

https://dx.doi.org/10.1007/s00231-019-02742-7

The accuracy of laser flash analysis explored by finite element method and numerical fitting

Alexandra Philipp[1], Jonas Eichinger[2,3], Roland C. Aydin[4], Argyrios Georgiadis[1], Christian J. Cyron[3,4], Markus Retsch[1*]

[1]University of Bayreuth, Department of Chemistry, Universitaetsstr. 30, 95447 Bayreuth, Germany
*E-mail: markus.retsch@uni-bayreuth.de, Phone: +49921 / 55-3920

[2]Technical University of Munich, Institute for Computational Mechanics, Boltzmannstr. 15, 85748 Garching b. Munich, Germany

[3]Institute of Continuum Mechanics, Hamburg University of Technology, Eissendorfer Str. 42 (M), 21073 Hamburg, Germany

[4]Institute of Materials Research, Materials Mechanics, Helmholtz-Zentrum Geesthacht, Max-Planck-Str. 1, 21502 Geesthacht, Germany

Abstract

Laser flash analysis (LFA) has become over the last decades a widely used standard technique to measure the thermal diffusivity of bulk materials under various conditions like different gases, atmospheric pressures, and temperatures. A curve fitting procedure forms the heart of LFA. This procedure bases on a mathematical model that should ideally account for inherent shortcomings of the experimental realization such as: duration of the heating pulse, heat losses to the environment and sample holder, non-opaque samples, and radiative heat transfer. The accuracy of the mathematical model and curve fitting algorithm underlying LFA defines an upper bound of the accuracy of LFA in general. Unfortunately, not much is known about the range of parameters and conditions for which this accuracy is acceptable. In this paper, we examine the limits of accuracy of LFA resulting from its underlying computational framework. To this end, we developed a particularly accurate and comprehensive computational framework and applied it to data from simulated experiments. We quantify the impact of different (simulated) experimental conditions on the accuracy of the results by comparing the fits results of our computational framework to the known simulation input parameters. This way we

demonstrate that a state-of-the-art computational framework for LFA admits determining thermal conductivities of materials in a broad range from at least 0.16 W/mK to 238 W/mK with relative errors typically well below 4 % even in the presence of common undesired experimental side effects.

1. Introduction

Laser flash analysis (LFA) is a simple and widely used technique for the determination of the thermal properties of solid samples with uniform thickness. LFA represents a transient characterization method and provides fast access to the thermal diffusivity of a given material. LFA has several advantages which have made this method increasingly popular since its invention more than 50 years ago: short measurement time, small sample size compared to steady-state methods, non-destructive measurement, assessment of temperature-, pressure-, gas composition-dependence, and high throughput. Additionally, it is possible to measure the specific heat capacity [1-10].

In a typical flash experiment, the front surface of the sample is heated by a short-duration light pulse created by a laser or flash lamp. The time-dependent temperature increase on the rear surface of the sample is measured by a contactless infrared detector. In an ideal adiabatic case, the thermal diffusivity α can be directly determined from the half-rise time $t_{1/2}$ using a formula derived by Parker *et al.* [1]:

$$\alpha = (1.38 \cdot L^2)/(\pi^2 \cdot t_{1/2}). \quad (1)$$

Here L is the thickness of the sample. Parker's model is only applicable in case of a negligibly short heat pulse that is uniformly irradiated as well as uniformly absorbed by the full front surface of the sample. Furthermore, the sample must be opaque (optically, to block the light flash and thermally, to prevent radiative heat transfer), isotropic, uniform in thickness, and thermally insulated from the environment. Parker *et al.* recommend a black coating of the sample's rear and front face to ensure a homogenous absorption of the heat pulse as well as to make the sample opaque [1].

Practically, an adiabatic measurement, as assumed implicitly in the derivation of Parker's formula, cannot be conducted, since thermal losses to the environment are inevitable. The time-dependent temperature on the rear sample surface deviates from Parker's ideal case due to such thermal losses. Instead of reaching a steady temperature plateau, the temperature decreases at

long measurement times and the half-rise-time shifts to lower times. Thus, the prefactor of 1.38 in Equation (1) and therefore Equation (1) as a whole is no longer valid [11].

To yet enable the applicability of the flash method under practical conditions, a host of theoretical models has been developed. These models consider heat losses due to radiation and/or natural convection [12-15,3,16-18]. In addition to heat loss effects, it can also be important to take the actual pulse length and shape into account. This is particularly relevant for thin samples and/or samples with a high thermal diffusivity, and consequently fast temperature diffusion. Thus, refinements to Parker's model have been developed, which consider the so-called finite pulse effect [19-22]. Ultimately, one needs to combine all loss mechanisms and the finite pulse lengths for a realistic description of actual measurements [23-25].

Radiative heat transfer leads to an additional and strong contribution to the effective temperature-time-curve in the case of (semi-)transparent samples. Examples of such materials are glasses or ceramics where heat is not only transferred through conduction but also *via* radiation, especially at high temperatures [26]. Also, porous materials at room temperature can be affected. Numerous research groups have focused on the physics of laser flash measurements of semi-transparent materials and enabled the correct determination of the thermal diffusivity of these materials [27-29,26,30-35].

The accuracy of the computational framework, that is, of the mathematical model and curve fitting algorithm, underlying LFA naturally defines an upper bound of the accuracy of LFA in general. This problem matters in particular if practical constraints result in experimental conditions which deviate from the ideal conditions assumed in the mathematical model of the experimental conditions underlying LFA. For example, these models typically assume cylindrical material samples, a complete sample surface illumination, and negligible heat losses through the sample holder whereas in practice these conditions can often not be ensured in experiments. The impact of such deviations from ideal experimental conditions on the accuracy of LFA remains poorly understood to date.

In this paper, we first introduce and describe in detail a state-of-the-art computational framework for LFA,, which is based on the equations of Parker *et al.* [1], Cape and Lehman [13], Dusza [25] and Blumm *et al.* [26] and which thus in general accounts at least to a certain extent for aspects such as thermal losses, finite pulse length and potential radiative contributions. For this state-of-the-art computational framework, we analyzed the associated inherent accuracy limitations, in particular, due to deviations from ideal experimental

conditions. To this end, we performed finite element simulations of laser flash experiments. The output data of these simulations were analyzed as usually experimental data in LFA. From the differences between the thermal conductivity values retrieved by such an inverse analysis and the original input parameters of the simulations, we could determine the inherent accuracy limitations of the employed computational framework and its sensitivity to deviations from ideal experimental conditions. This way we can conclude that a state-of-the-art computational framework for LFA admits – if considering only the error associated with the computational framework itself - measurement of thermal conductivity parameters in a broad range (at least 0.16 W/mK to 238 W/mK) with relative errors mostly well below 4 % even in the presence of common deviations from ideal experimental conditions.

2. Methods

2.1. Computational framework for LFA

Based on the work of Parker *et al.* [1], Cape and Lehman [13], Dusza [25] and Blumm *et al.* [26] we developed a new computational framework using the software package Matlab for computing the thermal diffusivity from temperature rise curves obtained from (real or simulated) laser flash measurements. Our framework includes multiple optional corrections terms, which can be switched on when using the framework (Figure 1). This way it is capable of calculating the thermal diffusivity under adiabatic as well as non-adiabatic conditions accounting also for radiative heat transfer if required. Finite pulse effects depending on the actual length and shape of the laser pulse can be considered. A pulse correction function of predefined shapes (exponential, triangular, linear-exponential) can be chosen, and the length of the pulse can be defined.

The following section briefly illustrates the basic equations of the developed framework for adiabatic and non-adiabatic boundary conditions and explains how they can be extended by optional correction terms to account for effects like radiative heat transfer.

The subsequent section describes key aspects that ensure the robustness and accuracy of our computational framework.

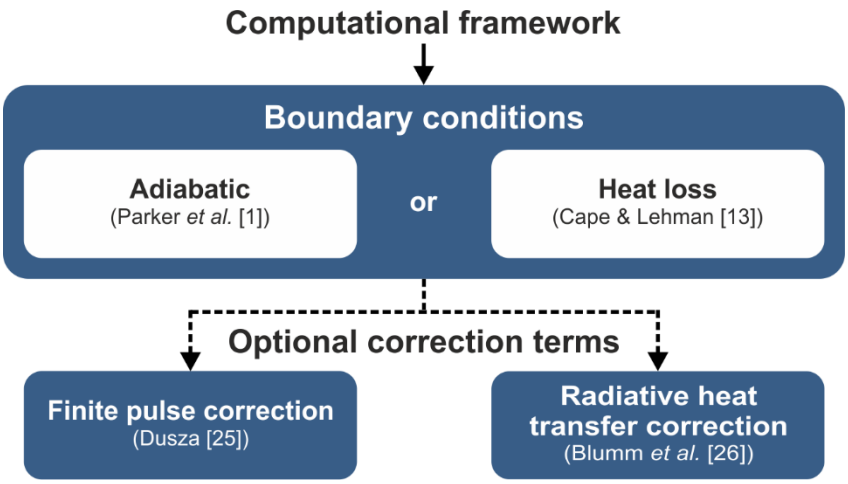

Fig 1 Overview of the computational framework. The basic form of the equation describing heat transfer in the sample is determined by the choice of boundary conditions. Either effects resulting from the finite laser pulse or radiative heat transfer can be considered by additional correction terms

2.1.1. Basic equations

Adiabatic conditions are assumed in our computational framework if the temperature decrease is less than 1 % in the last 20 % of the given temperature data points. In the adiabatic case, Parker's [1] temperature rise function

$$T^{A}(x = L, r = 0, t) = 1 + 2\sum_{i=1}^{\infty}(-1)^{i}\, e^{-\frac{i^2\pi^2\alpha t}{L^2}}, \tag{2}$$

with x being the distance from the front to the rear surface of the sample, L the sample length and t the time is used to determine the thermal diffusivity of a given sample material. To account for effects resulting from the laser flash impulse the model can be extended according to Dusza [25]:

$$T^{A,PSF}(x = L, r = 0, t) = P(1) + 2\sum_{i=1}^{\infty}(-1)^{i}\, e^{-\frac{i^2\pi^2\alpha t}{L^2}}\, P\left(-\frac{i^2\pi^2\alpha}{L^2}\right), \tag{3}$$

with P being a certain pulse shape function as defined by Dusza [25]. In case of very thin samples or samples with a high thermal diffusivity, often radiative heat transfer rather than finite pulse effects are considered, which leads according to Blumm *et al.* [26] to

$$T^{A,R}(x = L, r = 0, t) = \underbrace{1 + 2\sum_{i=1}^{\infty}(-1)^{i}\, e^{-\frac{i^2\pi^2\alpha t}{L^2}}}_{adiabatic\ heat\ transfer} + \underbrace{A + 2A\sum_{i=1}^{\infty} e^{-\frac{i^2\pi^2\alpha t}{L^2}}}_{radiative\ heat\ transfer} \tag{4}$$

with A being a factor that must be fitted describing effects of properties like the energy of the laser pulse.

As adiabatic conditions are experimentally barely realizable due to convection and radiation, Cape and Lehman [13] introduced a new model where they added heat loss correction terms to the method proposed by Parker *et al.* [1]. We will show in the following, that the model is also capable of yielding good results regarding additional loss mechanism that are unavoidably present in the experimental setup due to the sample holder and non-ideal sample geometry. Cape and Lehman [13] introduced the following model including terms describing heat losses to the environment:

$$T^{HL}(x = L, r = 0, t) = \sum_{m=0}^{\infty} C_m \, \xi_m \sum_{i=1}^{\infty} D_i(H_1) e^{(\omega_{im} t/t_c)} \tag{5}$$

with $C_m = (-1)^m \frac{2\xi_m}{{\xi_m}^2 + 2H_2 + {H_2}^2}$, $D_i(H_1) = \frac{2H_1}{({H_1}^2 + \lambda_i^2) J_0(\lambda_i)}$, $\omega_{im} = -(L/\pi)^2 \left(\frac{{\xi_m}^2}{L^2} + \frac{\lambda_i^2}{R_s^2} \right)$, $t_c = L^2/(\pi^2 \alpha)$ and λ_i being the solution of $H_1 J_0(\lambda_i) - \lambda_i J_1(\lambda_i) = 0$. J_0 and J_1 are the Bessel functions of the zeroth and first degree. ξ_m is the solution of

$$\left({\xi_m}^2 - {H_2}^2 \right) \tan(\xi_m) = 2\xi_m H_2. \tag{6}$$

Given that heat loss effects and finite pulse effects can be present simultaneously, Dusza [25] expanded the model of Cape and Lehman [13] by adding a pulse shape function adjustable to shape and length of the pulse used in the respective experiment:

$$T^{HL,PSF}(x = L, r = 0, t) = \sum_{m=0}^{\infty} C_m \, \xi_m \sum_{i=1}^{\infty} D_i(H_1) e^{(\omega_{im} t/t_c)} \, P(\omega_{im}/t_c) \tag{7}$$

with P being a pulse shape function as described by Dusza [25].

Analogously to the adiabatic case, transmitted radiation from the irradiated front surface to the detector can be incorporated into the model according to Blumm *et al.* [26]

$$T^{HL,R}(x = L, r = 0, t) = T^{HL}(x = L, r = 0, t) + \underbrace{A \sum_{m=0}^{\infty} C_{m,rad} \, \xi_m \sum_{i=1}^{\infty} D_i(H_1) e^{(\omega_{im} t/t_c)}}_{radiative\ heat\ transfer} \tag{8}$$

with

$$C_{m,rad} = \frac{2\xi_m}{{\xi_m}^2 + 2H_2 + {H_2}^2}. \quad (9)$$

In our computational framework, the user can choose initially which optional corrections (Figure 1) should be taken into account in the mathematical model used to fit a temperature rise data set.

2.1.2. Key mathematical aspects

Independently of the chosen equation we identified some crucial aspects to obtain a robust computational framework. In the following, we briefly summarize these crucial aspects. The code of our computational framework, as well as an exemplary input file, are provided in the Supplementary Material.

1) In case heat losses are considered when determining the thermal diffusivity of a sample material, the roots of Equation (6) must be calculated. Cape and Lehman [13] stated an approximate formula for the computation of these roots for cases where $H_2 < 1$. However, the formula was shown to be wrong by Josell *et al.* [18] who presented a corrected version. Unfortunately, in cases of Biot numbers $H_2 > 1$, also the solution of Josell *et al.* [18] yields wrong results. As we observed that Biot numbers $H_2 > 1$ may appear at least at some point during the iterative fitting process, the equations of Josell *et al.* alone are not sufficient for a robust algorithm.

To overcome this problem, we implemented a robust and efficient algorithm for finding all required roots of Equation (6) without restrictions regarding the Biot number H_2. The algorithms are based on an analytically gained understanding of how many roots must exist in certain subdomains. Most importantly it takes into consideration that two roots exist in the neighborhood of H_2 in case of $H_2 > \pi/2$, see Figure 2. Using both of these roots in Equations (5), (7), and (8) was identified to be crucial for accurate computation of the thermal diffusivity α.

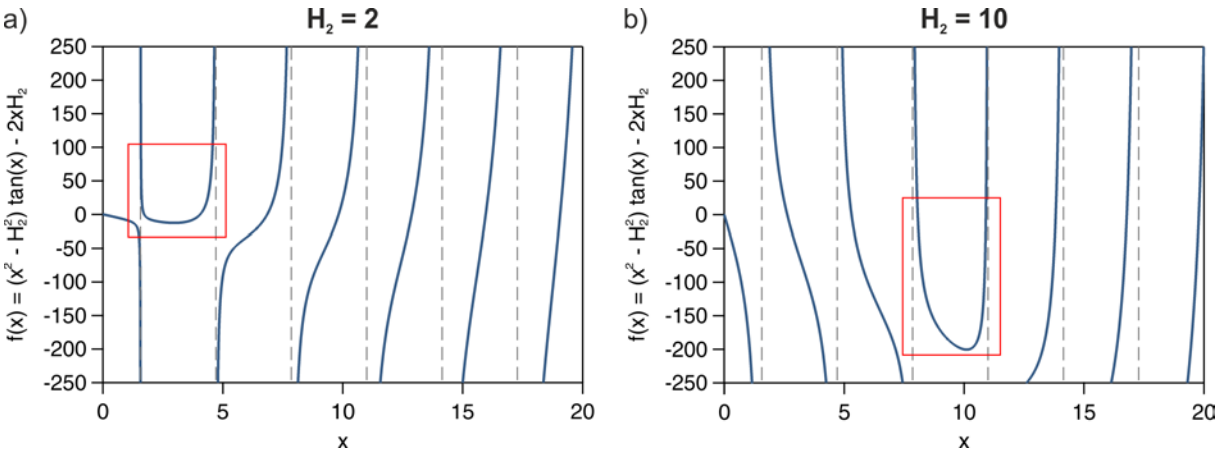

Fig. 2 Plot of Equation (6) for Biot numbers $H_2 > 1$: a) $H_2 = 2$, b) $H_2 = 10$. Red rectangles show critical intervals for numerical determination of roots

2) All temperature rise data obtained from experiments, or numeric simulations are normalized for a smoothed maximum temperature as well as shifted so that the temperature rise equals zero at time $t = 0$. In addition, all equations mentioned above describing the temperature rise at the rear surface of a sample are formulated for absolute temperature values and therefore have to be normalized in every iteration of the fitting process by the maximum temperature of the current iteration.

3) To ensure that our fitting algorithm yields parameters which represent a global optimum with respect to the quality of the fit, it is important to start the iterative calculations underlying to the fitting procedure with an initial guess sufficiently close to this global optimum. We found that equation (1) provides a suitable initial guess for the thermal diffusivity α.

4) If the half maximum time of a sample is larger than 100 times the length of the pulse, the pulse correction function is deactivated as the influence, in that case, is negligible. Parasitic effects in the curve fitting procedure were observed otherwise.

5) In case of heat loss boundary conditions, the specimen radius R_s can either be specified by a numeric value or fitted just like the thermal diffusivity α. The latter was found to be beneficial in case of an arbitrarily shaped sample geometry for which the exact sample radius is unknown.

7) Both the Levenberg-Marquard as well as the Trust-Region-Reflective algorithm as pre-implemented in Matlab were found to perform well for computing the best fit thermal diffusivity. In the computations performed for this paper, both worked equally robust.

2.2. Framework for simulation of experiments

To clarify the nomenclature used in this paper, we want to define the following terms: heat losses to the environment, radial losses, and facial losses.

Here, *heat losses to the environment* refer to radiative or convective heat losses from all external boundaries. *Radial losses* arise from an incomplete excitation of the lower sample surface by the heat pulse that leads to radial heat flow into the sample. If the sample is put on a sample holder, *facial losses* into the sample holder occur.

2.2.1. General setup

To quantify the accuracy of the computational framework used in LFA, we applied this framework to data from simulated rather than real experiments. The motivation of this approach is twofold. On the one hand, analyzing the data from simulated experiments has the advantage that the correct solutions for the parameters to be identified with the LFA framework are already known because they are simply the input parameters of the performed computer simulations. This enables a straightforward quantification of the error associated with the computational framework used in LFA. On the other hand, deviations from ideal experimental conditions can easily be mimicked and controlled in computer simulations so that their respective impact on the accuracy of LFA can be examined in detail. To simulate experiments, we performed time-dependent heat transfer simulations using the finite element (FE) software COMSOL Multiphysics®. To study the radial losses separately from the facial losses, two different geometries were chosen: a disk (Figure 3a) representing the sample and a disk on a sample holder (Figure 3b). In all our simulations we assumed axisymmetric geometries. The disk-shaped sample has a thickness of 1 mm and a radius R_{sample} of 5 mm.

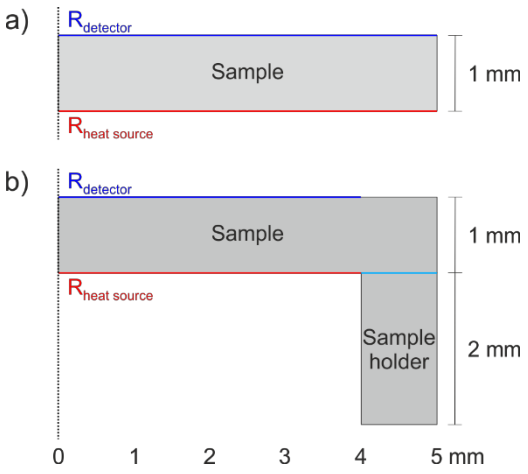

Fig. 3 General set-up **a** Simple case without sample holder and **b** geometry with a sample holder; the dotted

line at R=0 represents the axis of symmetry. The heat source is marked in red, the evaluation range in dark blue

A heat source in the form of a (temporally) triangular heat pulse with a pulse duration of $\tau =$ 2 ms was imposed on the lower edge of the sample disk (red line in Figure 3a and b). The intensity of the heat pulse was assumed to be uniform within a disk of radius $R_{heat\ source}$. We used various heat source radii $R_{heat\ source}$ for the investigation of radial heat losses into the sample using the geometry depicted in Figure 3a. A heat source radius of 5 mm corresponds to a complete excitation area (100 %) of the lower sample surface, 4 mm to an excitation area of 64 %, 3 mm to 36 %, and 1 mm to 4 %. Furthermore, we modeled radiative heat transfer using a second heat source imposed on the upper edge of the sample disk opposite the first heat source. To study the facial losses into the sample holder (Figure 3b), a heat source radius of 4 mm was used. These facial losses were adjusted by the magnitude of the thermal contact conductance at the interface between the sample and sample holder (light blue line in Figure 3b).

In adiabatic cases, i.e., without any heat losses to the environment, all external boundaries were assumed to be thermally insulating. In other studies, heat losses to the environment were considered, with heat loss boundary conditions being applied to all external boundaries.

We used sample materials covering a broad range of thermal conductivities (0.16 - 238 $Wm^{-1}K^{-1}$) to examine the applicability of the LFA procedure over a large parameter range. Due to its high thermal conductivity, copper was used as the material for the sample holder. The material parameters used for the simulations are listed in Table 1.

Table 1 Material parameters used for the FE simulations

Material	κ [$Wm^{-1}K^{-1}$]	C_p [$Jkg^{-1}K^{-1}$]	ρ [kgm^{-3}]	ε
Aluminum (Al)	238	900	2700	-
Titanium (Ti)	7.5	710	4940	-
Quartz (SiO_2)	1.4	730	2210	-
Polystyrene (PS)	0.16	1300	1050	0.9
Copper (Cu)	400	385	8700	0.05

κ: thermal conductivity, C_p: heat capacity at constant pressure, ρ: density, ε: emissivity

Mesh convergence tests were performed to ensure mesh size independent results (Figure S1, Supplementary Material). Furthermore, suitable time ranges and time steps of the solver were chosen for the different sample materials (Figure S2 and S3, Supplementary Material).

Subsequently, the time-dependent average temperature rise at the upper boundary of the sample was extracted from the simulation result. The radius of the region over which the temperature average was computed, i.e., the detector radius $R_{detector}$ (Figure 3a and b, blue line), was varied from 5 to 1 mm. This procedure mimics another experimental pre-requisite: confining the detection area to small radii allows measuring specimen, which are difficult to scale up and/or to produce with a high confidence regarding the sample thickness L. One should note that we determine the average temperature across the detector area, whereas the mathematical framework only considers the temperature in the center (r = 0). One can, therefore, expect that a higher deviation occurs for heat loss/detection area combinations that evoke large temperature gradients in the sample's top surface.

2.2.2. Numerical studies

- *Ideal adiabatic case and heat losses to the environment ($R_{heat\ source} = R_{sample}$)*

Firstly, the ideal adiabatic case was simulated for all samples to validate consistency between the FE method and the numerical fitting procedure. Thereby, the entire lower boundary of the disk-shaped sample (Figure 3a) was excited by a 2 ms heat pulse, and no heat losses were assumed to occur. Since adiabatic conditions cannot be realized experimentally, heat losses to the environment, i.e., thermal radiation and convection to air, were exemplarily modeled for polystyrene (PS). The heat loss boundary conditions were applied to all external boundaries. Results are summarized in Section 3.1.

- *Radial losses and radiative heat transfer ($R_{heat\ source} < R_{sample}$)*

The influence of radial losses into the sample, which arises from an incomplete excitation of the lower sample surface, was studied under adiabatic conditions using excitation areas smaller than 100 % of the lower sample surface. In addition to the excitation area, the detector radius was also varied. Experimentally, the detection area can be adjusted by differently sized sample apertures. Again, we used the geometry depicted in Figure 3a. Radiative heat transfer was simulated by introducing a second heat source on the upper sample surface. The amount of radiation was adjusted by the power of the heat source and varied between 0.25 – 2.5 % of the initial power. This study was only conducted for PS using an excitation area of 4 % and $R_{detector} = 1\ mm$. Results are summarized in Section 3.2.

- *Facial losses and heat losses to the environment ($R_{heat\ source} < R_{sample}$)*

Experimentally, if the sample is put on a sample holder (Figure 3b), radial losses are increased due to facial losses into the sample holder. Facial losses (without heat losses to the environment) were modeled using an excitation area of 64 %; different detector radii were used for the

evaluation. First, the thermal contact conductance between the sample and sample holder was varied exemplarily for PS. Then, the highest possible thermal contact conductance was applied to all materials. Finally, the most realistic case with facial losses as well as heat losses to the environment was modeled for PS. Results are summarized in Section 3.3.

2.2.3. Data evaluation

From the evaluation of the simulation results, temperature-rise-versus-time curves were obtained. First, we normalized the temperature values to the maximum temperature ($V = \Delta T/\Delta T_{max}$). Then, we interpolated the data using the software Igor Pro to obtain data points evenly spaced in time to avoid overweighting of specific time periods in the fitting due to increased density of interpolation points. This is necessary because finer time steps were used for the first part of the simulation. Negative time data was added as a baseline. Subsequently, we fitted the normalized temperature-rise-versus-time curves with the developed computational framework (Figure 1). A triangular pulse correction function and a pulse duration of 2 ms were used for all computations. As described above, in case of a negligible influence of pulse shape and duration, no pulse correction term is added to the equations to avoid parasitic effects during fitting. Dependent on the extent of temperature losses, equations considering either adiabatic or heat loss boundary conditions were used. Radiative heat transfer correction terms were accounted for in the fitting procedure in cases where part of the illumination flash was simulated to transmit to the top sample surface. The fit yields the thermal diffusivity α_{fit} that is used to calculate the thermal conductivity κ_{fit}:

$$\kappa_{fit} = \alpha_{fit} \cdot \rho \cdot C_p \tag{10}$$

where ρ is the density and C_p the specific heat capacity (Table 1). Then, the relative deviation of the thermal conductivity κ chosen as the input parameter for the respective simulation (Table 1) and the thermal conductivity κ_{fit} retrieved from an inverse analysis of the simulation output data was computed as

$$relative\ deviation = ((\kappa_{fit} - \kappa)/\kappa) \cdot 100\ \% \tag{11}$$

2.3. Experimental validation using xenon flash analysis

In this paper, we analyze the accuracy of LFA by applying the underlying computational framework to the output data of simulated experiments. We conclude that the underlying computational framework allows LFA with a relative error well below 4% for a large variety

of experimental conditions. To confirm this conclusion, we performed real experiments under varying conditions.

We performed thermal diffusivity measurements with an XFA500 xenon flash apparatus (Linseis), equipped with an InSb infrared detector. BCR-724 was used as a reference sample for the experimental study. The sample had a radius of 6.35 mm and a thickness of around 1.5 mm. The sample was coated with a thin graphitic layer on each side. The precise sample thickness was measured with a Litematic VL-50 (Mitutoyo). The graphite coating ensures a good absorbance of the xenon flash and a high IR emissivity. Different sample holders and covers were used to vary the excitation area and detection area, respectively. All measurements were performed in air and at room temperature (295 K). The obtained data were evaluated using the computational framework discussed above (with triangular pulse correction function, a pulse duration of 2 ms, no radiative heat transfer).

3. Results and discussion

3.1. Ideal adiabatic case and influence of heat losses to the environment

The ideal adiabatic case was simulated for all sample materials. Here, the sample geometry depicted in Figure 3a was used. The complete lower sample surface was excited by a short heat pulse, and no heat losses to the environment were considered. Thus, purely one-dimensional heat transfer in the thickness direction of the sample occurs. Figure 4a shows the resulting temperature rise versus time curves. In general, the temperature increases with time until a plateau is reached. As expected, the half-time shifts to longer times for samples with low thermal conductivity.

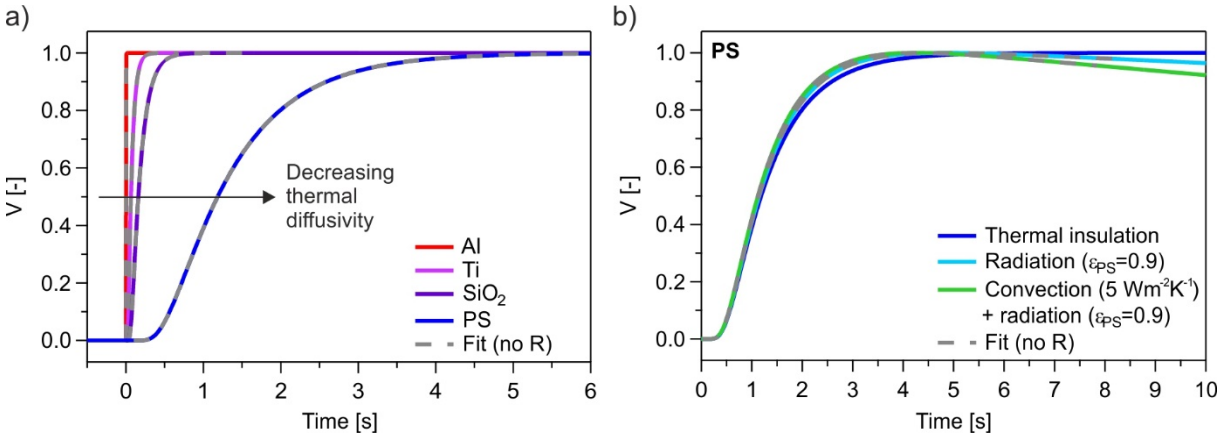

Fig. 4 Normalized temperature-rise-versus-time curves and corresponding fits **a** Ideal adiabatic case without losses **b** Influence of heat losses on the normalized temperature-rise-versus-time curve for PS

We used the computational framework from Section 2.1.1 to extract the thermal diffusivity from the simulation data. The corresponding fits are also shown in Figure 4a (grey dashed lines). As can be seen, they fit the simulated curves perfectly. In Table 2, the obtained thermal diffusivity α_{fit}, the calculated thermal conductivity κ_{fit}, the reference value κ, and the calculated relative deviation are listed. Relative deviations on the order of 0.1 % were obtained for all materials. Thus, the developed computational framework is applicable even for highly conducting materials like Al, where the finite pulse correction is important (pulse duration: 2ms, half-time: 2.45 ms).

Table 2 Fitting results of the temperature-rise-versus-time curves for the ideal adiabatic case (Figure 4a) in comparison to the input values

	Combined fit		Input	*Rel. dev. [%]*
	α_{fit} *[cm²s⁻¹]*	κ_{fit} *[Wm⁻¹K⁻¹]*	κ *[Wm⁻¹K⁻¹]*	
Al	0.980709	238	238	0.13
Ti	0.021418	7.51	7.50	0.16
SiO_2	0.008704	1.40	1.40	0.30
PS	0.001172	0.160	0.160	-0.01

α_{fit}: fitted thermal diffusivity, κ_{fit}: thermal conductivity calculated from α_{fit}, κ: input thermal conductivity.

In Figure 4b, the ideal adiabatic curve of PS is compared to more realistic cases. We introduced heat losses due to thermal radiation (solid light blue line) which occur under vacuum conditions. In the air, radiation and natural convection (solid light green line) lead to heat losses during the experiment. Because of these heat losses, the half-time shifts to slightly shorter times and the temperature decreases after reaching a maximum. The effect of heat losses to the environment is small since there is only a small temperature difference between the sample and the surrounding (room temperature). Furthermore, short measurement time and thin sample thickness are used. Again, the fitted results are in very good agreement with the simulation curves (Figure 4b, grey dashed line). This results in negligible relative deviations of the thermal conductivity (Table 3).

Table 2 Relative deviation of the thermal conductivity fitting results of PS with heat losses (Figure 2b) from the input parameters used in the FEM simulation.

	Thermal insulation	*Radiation*	*Convection + radiation*
PS	-0.01 %	-0.10 %	-0.18 %

Thus, by exciting the total surface area and measuring in air or vacuum at room temperature, one can expect to obtain very good fits for the thermal conductivity with negligible relative deviations from the real values due to the computational framework used for evaluation of the experimental data.

3.2. Radial losses and radiative heat transfer

An incomplete excitation of the lower sample surface by the heat pulse leads to radial heat flow into the sample. These radial losses increase with decreasing excitation area as shown in Figure 5a. To study the influence of radial losses into the sample due to an incomplete excitation, the geometry depicted in Figure 3a was used. The heat source and detector radius were varied from 4 mm to 1 mm. The different detection areas are marked in grey in Figure 5a. No heat losses to the environment were considered.

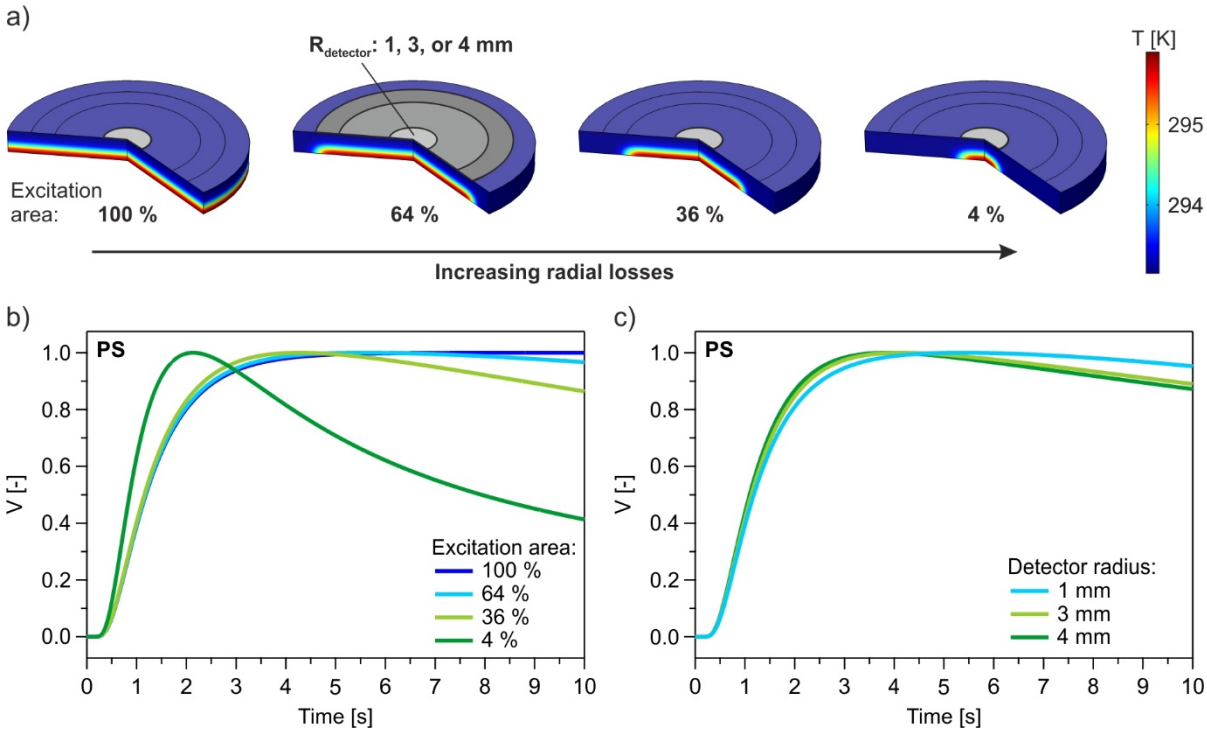

Fig. 5 Influence of radial losses **a** COMSOL images for different excitation areas. Radial losses arise from an incomplete excitation of the sample surface and increase with decreasing excitation area. No radial losses are

present for a complete excitation. **b,c** Normalized temperature-rise-versus-time curves are exemplarily shown for PS **b** Influence of the excitation area ($R_{detector}$: 1 mm). **c** Influence of the detector radius (excitation area: 64 %)

In Figure 5b, the normalized temperature rise versus time curves for different excitation areas are exemplarily shown for PS. For the evaluation, a detector radius of 1 mm was used. Similar to the heat losses to the environment, the radial losses into the sample lead to a decrease in the temperature after reaching a maximum value and the half-time shifts to lower times. The stronger the radial losses, the more pronounced are these changes. Besides the excitation area, we also studied the influence of the detector radius. The resulting curves for an excitation area of 64 % and different detector radii are again exemplarily plotted for PS (Figure 5c). The strongest temperature decrease after the maximum is obtained for a detector radius that is equal to the excitation radius (4 mm). The smaller the detector radius (compared to the excitation radius), the lower is the influence of the radial losses.

In Figure 6, the relative deviation of all materials is plotted against the excitation area. The used detector radius is depicted as differently sized circles; a small circle represents a small detection area and vice versa. Relative deviations from the input value below 4 % were obtained for all configurations, except for the material with the highest thermal conductivity and the highest radial losses (5.6 %). Thus, the combined fitting model leads to reliable results, especially for low conductive materials, even with radial losses present.

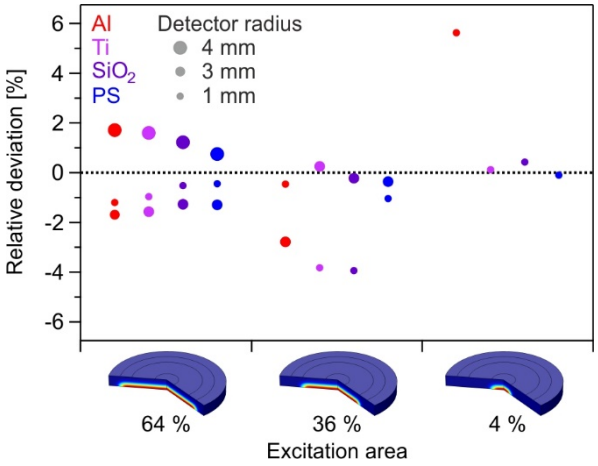

Fig. 6 Influence of radial losses: Relative deviation in dependence on the excitation and detection area

If the sample is not completely opaque to the excitation source (e.g., laser or xenon lamp) or it exhibits a porous structure, the light energy is not only absorbed at the lower sample surface but in the entire sample volume or at the upper sample surface. This leads to a sharp temperature

peak at $t \approx 0$ ms. To obtain reliable fitting results, this radiative heat transfer has to be considered in the fitting procedure. Here, in addition to radial losses, the influence of radiative heat transfer was studied using a second heat source on the upper sample surface (Figure 7a). This study was only conducted for PS using the smallest excitation area (4 %) and detector radius (1 mm), i.e., the most demanding specimen geometry regarding radial losses.

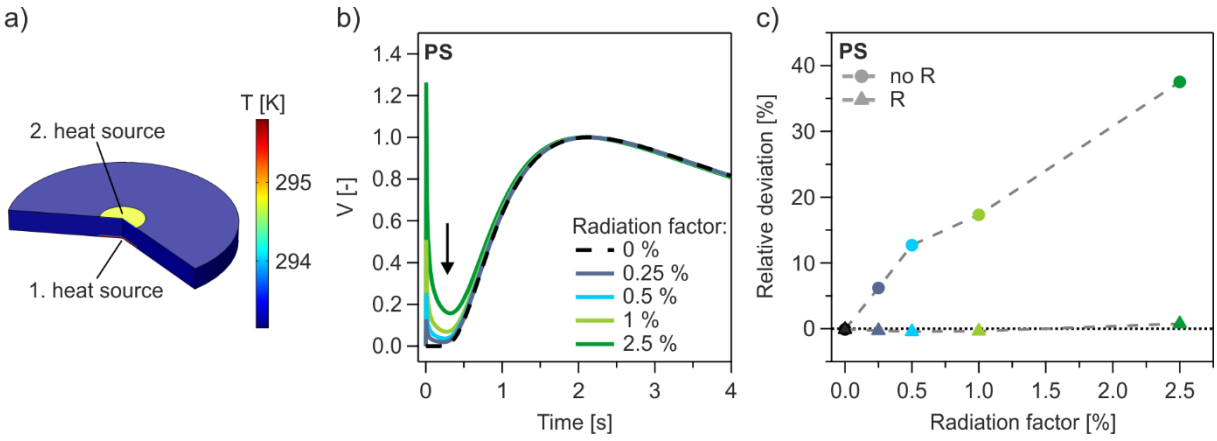

Fig. 1 Influence of radiative heat transfer **a** COMSOL snapshot at $t = 1$ ms illustrates the second heat source on the upper sample surface (excitation area: 4 %) **b** Normalized temperature-rise-versus-time curves of PS with radiative heat transfer. The jump in the temperature evolution is highlighted by an arrow **c** Comparison of the relative deviation obtained from the fit with ("R") and without ("no R") correction for radiative heat transfer.

The temperature-rise-time-curves for different radiation factors are compared in Figure 7b. The temperature at $t \approx 0$ ms rises when the radiation factor is increased. Also, the temperature after this initial peak increases and the half-time shifts to lower times. These changes lead to inaccurate results in case of fitting without corrections for radiative heat transfer. For the lowest radiation factor, a relative deviation above 6 % is obtained, which increases up to around 38 % for the highest radiation factor. In contrast, fitting with corrections for radiative heat transfer yields negligible relative deviations for all studied radiation factors combined with high radial losses due to an incomplete excitation. Thus, in this case, radiative heat transfer has to be considered in the fitting model.

3.3. Facial losses and influence of heat losses

By adding a sample holder to the geometry (Figure 3b) and enabling the heat flow through the sample/sample holder interface, facial losses into the sample holder occur and consequently enhance the radial losses. The direction of heat flow is illustrated by arrows in Figure 8a.

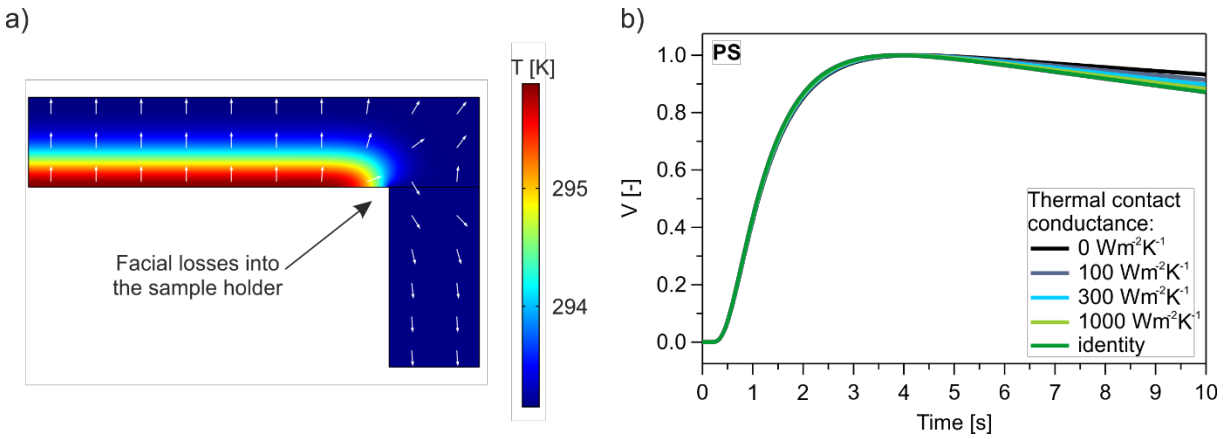

Fig. 8 Influence of facial losses **a** COMSOL image illustrating facial losses into the sample holder, arrows display the direction of heat flow **b** Normalized temperature-rise-versus-time curves of polystyrene for different thermal contact conductances (excitation area: 64 %, $R_{detector}$: 4 mm). No facial losses occur at a thermal contact conductance of 0 $Wm^{-2}K^{-1}$, while the maximum heat flow into the holder is present at the identity boundary condition

We performed the simulations for an excitation area of 64 %. The thermal contact conductance between the sample and the copper sample holder was varied from zero (no facial losses) to identity (maximum facial losses). In Figure 8b, the corresponding normalized temperature-rise-versus-time curves for a detector radius of 4 mm are exemplarily plotted for PS. The temperature after reaching the maximum value drops to a lower value as the thermal contact conductance increases. However, this is a rather small effect compared to the influence of the radial losses. This effect is even smaller for smaller detector radii. The corresponding relative deviations of all curves are below 1 % (Figure 9a).

Similar simulations were performed for all the other samples using the same detector radius and the maximum thermal contact conductance. As can be seen from Figure 9b, relative deviations below 3 % are obtained for all materials. Thus, one can conclude that facial losses into the sample holder are insignificant even for materials with high thermal conductivity.

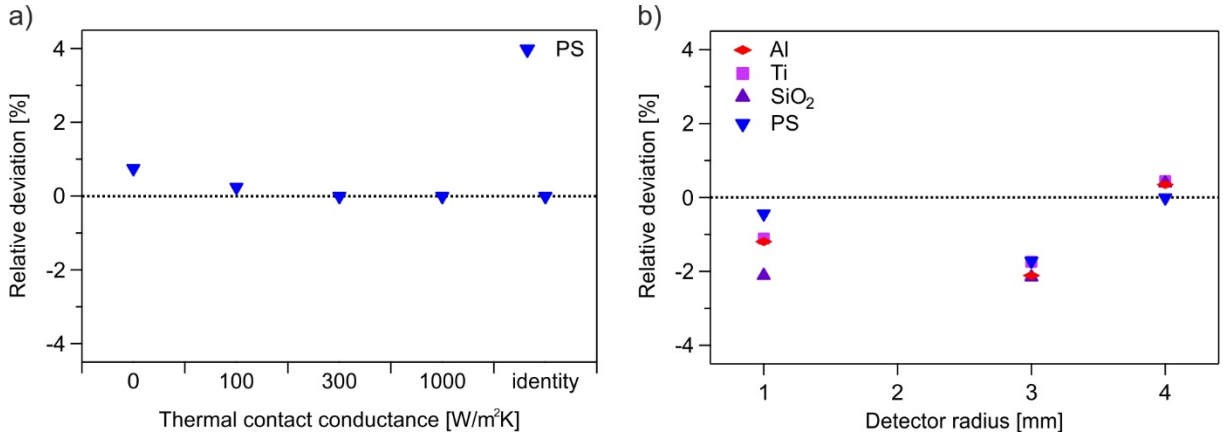

Fig 2 Influence of facial losses **a** Relative deviation of the thermal conductivity of PS obtained from fit and the preset thermal conductivity for different thermal contact conductance values **b** Relative deviation of all samples for maximum facial losses (identity boundary condition)

Heat losses are always present. Therefore, we studied the combined influence of all heat loss types: radiation, convection, and conduction into the sample holder (Figure 10a). Again, we chose PS as the material. Relative deviations below 2 % were obtained for all investigated configurations (Figure 10b). Furthermore, there are almost no differences between the relative deviation obtained from the simulation with thermal insulation and with heat losses.

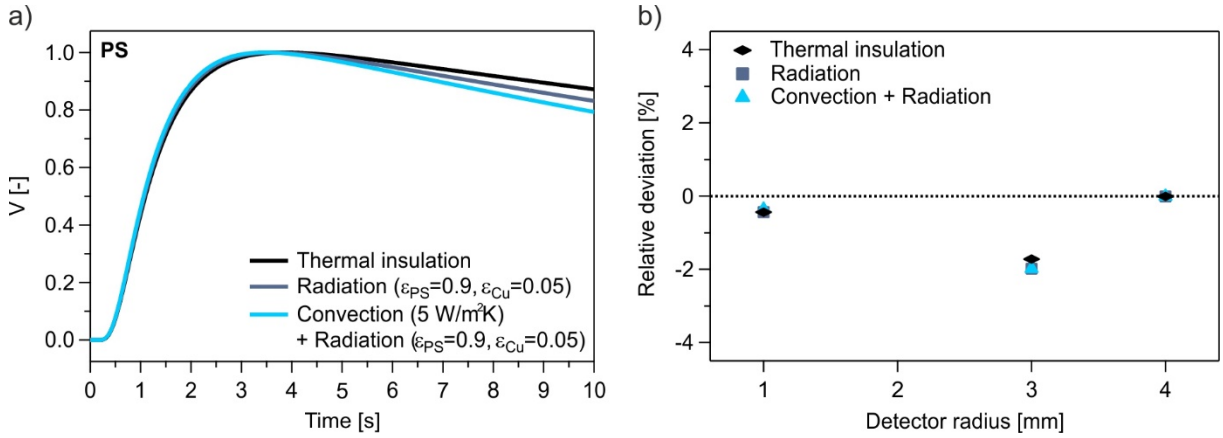

Fig. 10 a Normalized temperature rise versus time curves for PS with and without heat losses (detector radius: 4mm) **b** Relative deviation obtained for no heat losses and with heat losses due to radiation or convection as well as radiation

Our results demonstrate the remarkable robustness of the laser flash method to yield accurate values of the thermal diffusivity even for experimental conditions, which substantially deviate from optimal measurement conditions. This is a very positive result as it corroborates the confidence in thermal diffusivity results reported from laser flash analysis.

3.4. Experimental validationA

In the above sections we concluded by means of simulated experiments that the computational framework of LFA enables high accuracy measurements for a large variety of experimental conditions. To confirm this conclusion experimentally, we measured a reference sample (BCR-724 with certified thermal diffusivity value) using a xenon flash apparatus. Thereby, we used different sample holders to vary the excitation area (100 % - 10 %) and different sample covers to adjust the detection area (40 % - 10%). The received raw data and the corresponding fit (solid black line) are shown in Figure 11a. A reduction in the excitation or detection area leads to a lower maximum temperature rise. The fitted thermal diffusivity agrees very well with the certified thermal diffusivity of BCR-724 (Figure 11b) independently of the chosen sample holder/cover. This confirms our expectation from FE modeling that the computational framework underlying LFA is – if based on a state-of-the-art mathematical model – fairly robust to deviations from ideal experimental conditions . Forwhereas the measured raw data of the overall temperature increase (reflected by the voltage change of the InSb detector) vary significantly depending on the experimental conditions, the thermal diffusivity was consistently and correctly fitted.

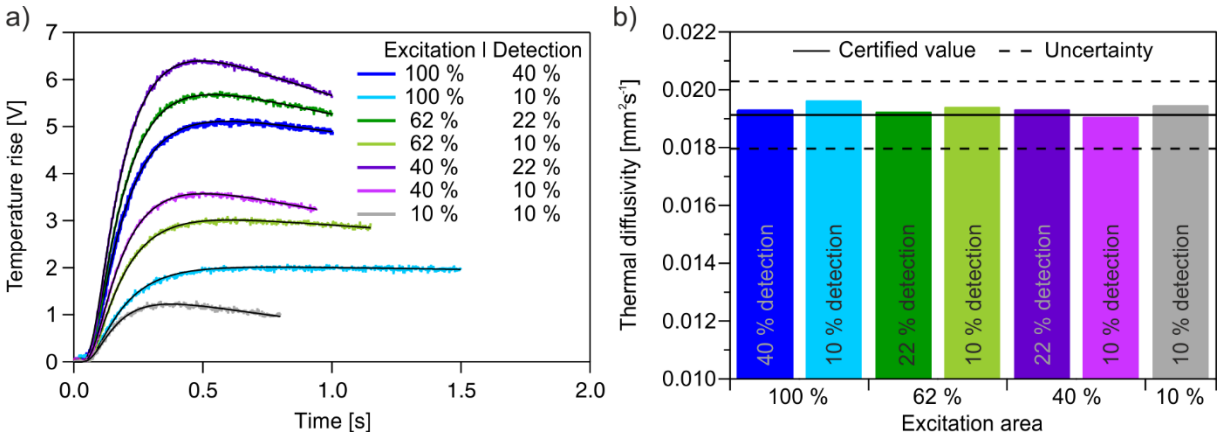

Fig. 3 a Temperature-rise-versus-time curves obtained from XFA measurements of BCR-724 and corresponding fit (solid black line) **b** Thermal diffusivity of BCR-724 measured using different sample holders and covers; the solid black line represents the certified value of BCR-724, the dashed black lines the upper/lower limit of the uncertainty range

3. Conclusion

The computational framework (i.e., mathematical model and fitting procedure) underlying laser flash analysis (LFA) naturally limits the accuracy of LFA. So far, the impact of this limitation is poorly understood. To quantify this impact, we developed a state-of-the-art computational framework for LFA based on the work of Parker *et al.* [1], Cape and Lehman [13], Dusza [25] and Blumm *et al.* [26]. This framework can account for heat losses to the environment, radial losses within the sample, facial losses into the sample holder, radiative heat transfer, as well as combinations of these processes. It operates robustly even for Biot numbers $H_2 > 1$.

We applied this state-of-the-art computational framework to analyze the output data of experiments. Thereby we focused on simulated rather than real experiments. We did so for two reasons. First, for simulated experiments, the error that results from the computational framework underlying LFA can easily and accurately be quantified. It is the difference between the known simulation input parameters and the parameter values which the computational framework yields when applied in an inverse analysis of the simulation output data. The second reason why we used simulated rather than real experiments is that in computer simulations different experimental conditions can easily be mimicked and controlled so that the impact of deviations from ideal experimental conditions can be examined conveniently. Our computational studies revealed that a state-of-the-art computational framework for LFA as we used it herein allows a determination of thermal conductivities for a broad range of materials and experimental conditions with a relative error of typically less than 4 %. This result confirms that LFA is a robust and reliable method for determining thermal diffusivity of materials even if an ideal sample preparation is practically in certain cases not possible.

Acknowledgments

This project was funded by the Lichtenberg Professorship provided by the Volkswagen Foundation.

References

1. Parker WJ, Jenkins RJ, Butler CP, Abbott GL (1961) Flash method of determining thermal diffusivity, heat capacity, and thermal conductivity. Journal of Applied Physics 32 (9):1679-1684. doi:doi:http://dx.doi.org/10.1063/1.1728417

2. Righini F, Cezairliyan A (1973) Pulse method of thermal diffusivity measurements. High Temperatures-High Pressures 5:481-501

3. Degiovanni A (1977) Diffusivité et méthode flash. Revue générale de thermique 185:420-442

4. Taylor RE (1979) Heat-pulse thermal diffusivity measurements. High Temperatures-High Pressures 11 (1):43-58

5. Balageas DL (1989) Thermal diffusivity measurement by pulsed methods. High Temperatures-High Pressures 21:85-96

6. Maglić K, Taylor R (1992) The apparatus for thermal diffusivity measurement by the laser pulse method. In: Compendium of thermophysical property measurement methods. Springer, pp 281-314

7. Sheindlin M, Halton D, Musella M, Ronchi C (1998) Advances in the use of laser-flash techniques for thermal diffusivity measurement. Review of Scientific Instruments 69 (3):1426-1436. doi:10.1063/1.1148776

8. Baba T, Ono A (2001) Improvement of the laser flash method to reduce uncertainty in thermal diffusivity measurements. Measurement Science and Technology 12 (12):2046

9. Vozár L (2001) Flash Method for thermal diffusivity measurement: Theory and Praxis. Constantine the Philosopher University,

10. Vozár L, Hohenauer W (2004) Flash method of measuring the thermal diffusivity. A review. High Temperatures-High Pressures 36 (3):253-264

11. Mendelsohn AR (1963) The effect of heat loss on the flash method of determining thermal diffusivity. Applied Physics Letters 2 (1):19-21. doi:doi:http://dx.doi.org/10.1063/1.1753717

12. Cowan RD (1963) Pulse method of measuring thermal diffusivity at high temperatures. Journal of Applied Physics 34 (4):926-927. doi:doi:http://dx.doi.org/10.1063/1.1729564

13. Cape JA, Lehman GW (1963) Temperature and finite pulse-time effects in the flash method for measuring thermal diffusivity. Journal of Applied Physics 34 (7):1909-1913. doi:doi:http://dx.doi.org/10.1063/1.1729711

14. Watt DA (1966) Theory of thermal diffusivity by pulse technique. British Journal of Applied Physics 17 (2):231

15. Clark III LM, Taylor RE (1975) Radiation loss in the flash method for thermal diffusivity. Journal of Applied Physics 46 (2):714-719. doi:doi:http://dx.doi.org/10.1063/1.321635
16. Degiovanni A (1985). High Temperatures-High Pressures 17:683-689
17. Balageas DL (1982) Nouvelle méthode d'interprétation des thermogrammes pour la détermination de la diffusivité thermique par la méthode impulsionnelle (méthode « flash »). Revue de Physique Appliquée 17 (4):227-237. doi:10.1051/rphysap:01982001704022700
18. Josell D, Warren J, Cezairliyan A (1995) Comment on ‘‘Analysis for determining thermal diffusivity from thermal pulse experiments’’. Journal of Applied Physics 78 (11):6867-6869. doi:10.1063/1.360452
19. Larson KB, Koyama K (1967) Correction for finite-pulse-time effects in very thin samples using the flash method of measuring thermal diffusivity. Journal of Applied Physics 38 (2):465-474. doi:10.1063/1.1709360
20. Taylor RE, Clark III LM (1974) Finite pulse time effects in flash diffusivity method. High Temperatures-High Pressures 6:65-72
21. Azumi T, Takahashi Y (1981) Novel finite pulse-width correction in flash thermal diffusivity measurement. Review of Scientific Instruments 52 (9):1411-1413. doi:10.1063/1.1136793
22. Xue J, Liu X, Lian Y, Taylor R (1993) The effects of a finite pulse time in the flash thermal diffusivity method. International Journal of Thermophysics 14 (1):123-133. doi:10.1007/bf00522666
23. Heckman RC (1973) Finite pulse-time and heat-loss effects in pulse thermal diffusivity measurements. Journal of Applied Physics 44 (4):1455-1460. doi:10.1063/1.1662393
24. Lechner T, Hahne E (1993) Finite pulse time effects in flash diffusivity measurements. Thermochimica Acta 218:341-350. doi:10.1016/0040-6031(93)80434-c
25. Dusza L (1995) Combined solution of the simultaneous heat loss and finite pulse corrections with the laser flash method. High Temperatures-High Pressures 27/28 (5):467-473
26. Blumm J, Henderson J, Nilsson O, Fricke J (1997) Laser flash measurement of the phononic thermal diffusivity of glasses in the presence of ballistic radiative transfer. High Temperatures-High Pressures 29:555-560. doi:10.1068/htec141
27. Tischler M, Kohanoff JJ, Rangugni GA, Ondracek G (1988) Pulse method of measuring thermal diffusivity and optical absorption depth for partially transparent materials. Journal of Applied Physics 63 (5):1259-1264. doi:10.1063/1.339950
28. Araki N (1990) Effect of radiation heat transfer on thermal diffusivity measurements. International Journal of Thermophysics 11 (2):329-337. doi:10.1007/bf01133565

29. Andre S, Degiovanni A (1995) A theoretical study of the transient coupled conduction and radiation heat transfer in glass: phonic diffusivity measurements by the flash technique. International Journal of Heat and Mass Transfer 38 (18):3401-3412. doi:https://doi.org/10.1016/0017-9310(95)00075-K

30. Hofmann R, Hahn O, Raether F, Mehling H, Fricke J (1997) Determination of thermal diffusivity in diathermic materials by the laser-flash technique. High Temperatures-High Pressures 29 (6):703-710. doi:10.1068/htrt115

31. Hahn O, Raether F, Arduini-Schuster MC, Fricke J (1997) Transient coupled conductive/radiative heat transfer in absorbing, emitting and scattering media: application to laser-flash measurements on ceramic materials. International Journal of Heat and Mass Transfer 40 (3):689-698. doi:https://doi.org/10.1016/0017-9310(96)00137-8

32. Andre S, Degiovanni A (1998) A new way of solving transient radiative-conductive heat transfer problems. Journal of Heat Transfer 120 (4):943-955. doi:10.1115/1.2825914

33. Mehling H, Hautzinger G, Nilsson O, Fricke J, Hofmann R, Hahn O (1998) Thermal diffusivity of semitransparent materials determined by the laser-flash method applying a new analytical model. International Journal of Thermophysics 19 (3):941-949. doi:10.1023/a:1022611527321

34. McMasters RL, Beck JV, Dinwiddie RB, Wang H (1999) Accounting for penetration of laser heating in flash thermal diffusivity experiments. Journal of Heat Transfer 121 (1):15-21. doi:10.1115/1.2825929

35. Lazard M, André S, Maillet D, Degiovanni A (2000) Radiative and conductive heat transfer: a coupled model for parameter estimation. High Temperatures--High Pressures(UK) 32 (1):9-17

The accuracy of laser flash analysis explored by finite element modeling and numerical fitting

Alexandra Philipp[1], Jonas Eichinger[2,3], Roland C. Aydin[4], Christian J. Cyron[3,4], Markus Retsch[1*]

[1]University of Bayreuth, Department of Chemistry, Universitaetsstr. 30, 95447 Bayreuth, Germany
*E-mail: markus.retsch@uni-bayreuth.de, Phone: +49921 / 55-3920

[2]Technical University of Munich, Institute for Computational Mechanics, Boltzmannstr. 15, 85748 Garching b. Munich, Germany

[3]Institute of Continuum Mechanics, Hamburg University of Technology, Eissendorfer Str. 42 (M), 21073 Hamburg, Germany

[4]Institute of Materials Research, Materials Mechanics, Helmholtz-Zentrum Geesthacht, Max-Planck-Str. 1, 21502 Geesthacht, Germany

Supplementary Material

1. Finite element modeling

Mesh convergence test

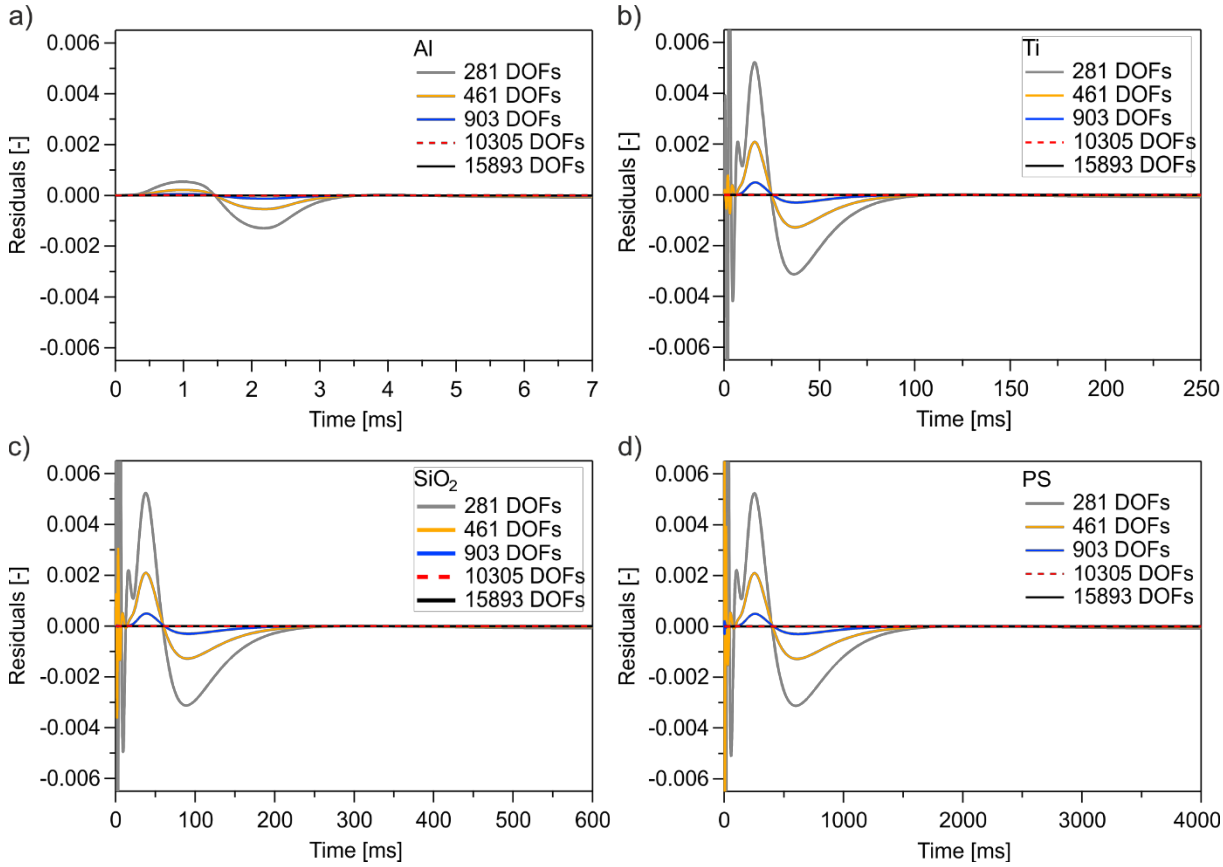

Fig. S1 For the mesh convergence tests, the geometry without sample holder (Figure 3a) and a heat source radius of 1 mm were used, whereas the number of mesh elements was varied. The time-dependent temperature increase for a detector radius of 1 mm was evaluated. Finally, the residuals compared to the finest mesh (15983 DOFs, black straight line) were calculated. Since there are no significant differences between the mesh with 10305 DOFs (dashed red line) and the finest mesh, a mesh with 10305 DOFs was used for all simulations (and samples)

Convergence test of time steps

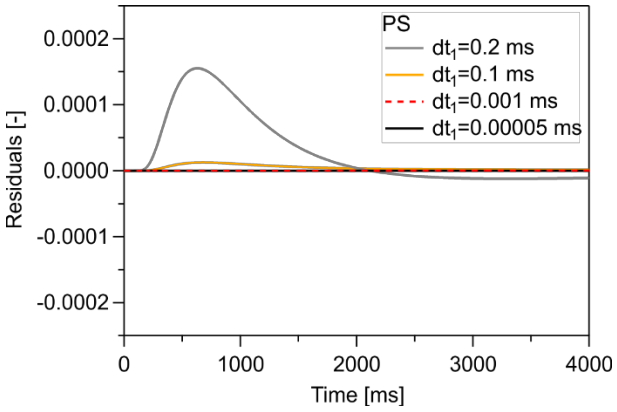

Fig. S2 Besides the mesh size, the time steps used for the time-dependent simulations are also necessary to adjust fine enough, especially in the time range of the 2 ms triangular heat pulse. For the convergence tests, again the geometry without sample holder (Figure 3a) and a heat source radius of 1 mm was used. The time-dependent temperature increase for a detector radius of 1 mm was evaluated. Here, exemplarily shown for PS, the time steps within the first 2 ms were varied and the residuals compared to the smallest time steps were calculated. For PS, 0.001 ms time steps for the first 2 ms were used for all simulations.

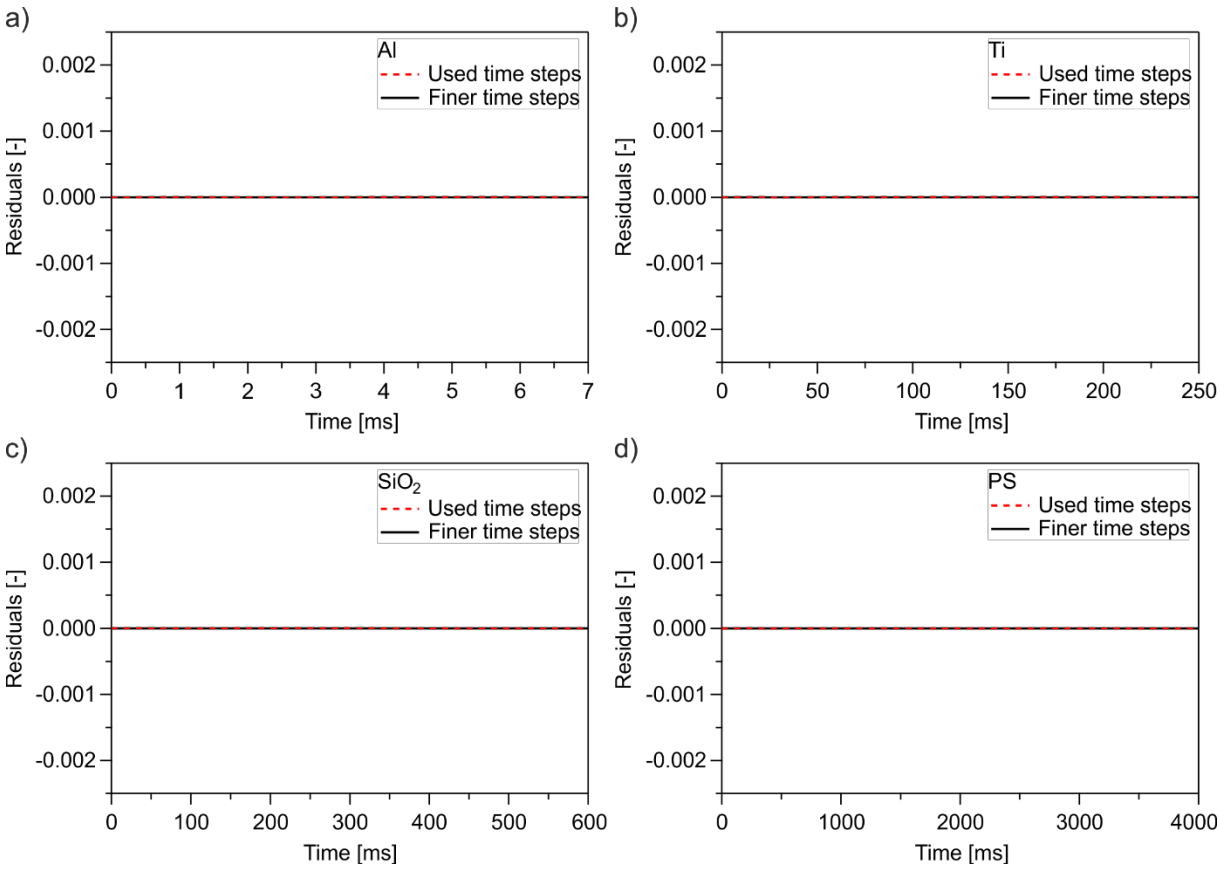

Fig. S3 For the convergence tests, again the geometry without sample holder (Figure 3a) and a heat source radius of 1 mm was used. The time-dependent temperature increase for a detector radius of 1 mm was evaluated and the residuals compared to the smallest time steps (black straight line) were calculated. Since there are no significant differences between the two curves, the used time steps (red dashed line) are chosen fine enough

Radial losses into the sample

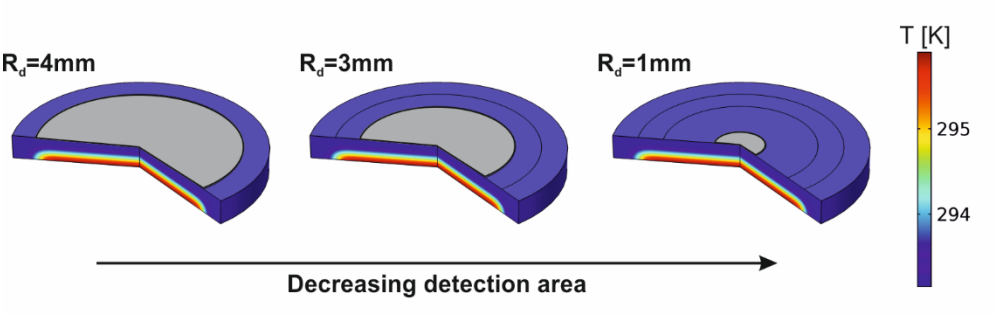

Fig. S4 Influence of radial losses: COMSOL images for the same excitation area, but different detector radii. The smaller the detector radius, the smaller the detection area

Influence of measurement time

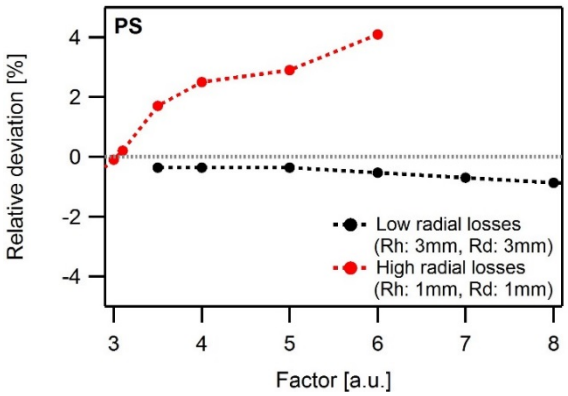

Fig. S5 Exemplary plot of relative deviation versus factor (factor times the half-time $t_{1/2}$). In the case of low radial losses, the fit will also lead for longer measurement times to good results (relative deviation < 1 %). However, for high radial losses, long measurement times increase the relative deviation. Thus, to obtain always the smallest error, short measurement times should be used in any case (low or high radial losses)